

## An investigation into the stresses in double-lap adhesive joints with laminated composite adherends

M.Y. Tsai<sup>a,\*</sup>, J. Morton<sup>b</sup>

<sup>a</sup> Department of Mechanical Engineering, Chang Gung University, Kwei-Shan, Tao-Yuan 333, Taiwan, ROC

<sup>b</sup> Department of Engineering Science, University of Oxford, Parks Road, Oxford OX1 3PJ, UK

### ARTICLE INFO

#### Article history:

Received 22 April 2010

Received in revised form 15 July 2010

Available online 15 August 2010

#### Keywords:

Double-lap joint

Adhesive

Adherend

Laminated composites

Stress analysis

Moiré interferometry

### ABSTRACT

The mechanics of double-lap joints with unidirectional ( $[0_16]$ ) and quasi-isotropic ( $[0/90/-45/45]_{2S}$ ) composite adherends under tensile loading are investigated experimentally using moiré interferometry, numerically with a finite element method and analytically through a one-dimensional closed-form solution. Full-field moiré interferometry was employed to determine in-plane deformations of the edge surface of the joint overlaps. A linear-elastic two-dimensional finite element model was developed for comparison with the experimental results and to provide deformation and stress distributions for the joints. Shear-lag solutions, with and without the inclusion of shear deformations of the adherend, were applied to the prediction of the adhesive shear stress distributions. These stress distributions and mechanics of the joints are discussed in detail using the results obtained from experimental, numerical and theoretical analyses.

Crown Copyright © 2010 Published by Elsevier Ltd. All rights reserved.

### 1. Introduction

Adhesively bonded joints have the potential to replace conventional fastener and rivet joints, especially in laminated composite structures. Adhesive bonding has merits over other jointing methods through the avoidance of drilled holes and the reduction of stress concentrations (Tong and Soutis, 2003). The double-lap adhesive joint is a simple configuration with relatively low peel stresses, so it is often used in determining the adhesive properties for stress analyses and material quality assurance (such as the ASTM D3528 test standard), and in structural bonding configurations.

The most widely-used stress analysis of double-lap joints is the classical Volkersen/de Bruyne solution which was developed by de Bruyne (1944) using Volkersen's single-lap theory (Volkersen, 1938). This solution is a shear-lag approach based on modelling the adherends as bars (without shear deformation) and the adhesive layer as a shear spring carrying only the shear stresses needed to transfer the longitudinal forces from the inner to the outer adherends. Later, Tsai et al. (1998) proposed an improved solution by including shear deformations in the adherend. For the design of double-lap joints with composite laminates, a method based on two stress-singularity parameters has been proposed for predicting the fatigue strengths of adhesively bonded single-step double-lap joints (Ishii et al., 1999). New designs of double-lap joints have

been proposed for adhesively bonding thick composite laminates by selecting ratios of the shear to normal stresses in the adhesive layers. The stress concentrations in the adherend surface plies and the adhesive layer at the leading edges of the doublers can be significantly reduced (Bahei-El-Din and Dvorak, 2001). A modification of Hashin's variational method for orthogonally cracked composite laminates has been applied in the stress analysis of a double-strap joint to obtain a simple analytical expression and an equivalent spring constant for the joint (Chalkley and Rose, 2001). More recently, a semi-analytical solution, including linearly elastic and bilinear adhesive behaviour, was developed for a geometrically nonlinear three-dimensional analysis of single- and double-lap tapered composite joints (Oterkus et al., 2006).

Finite element analysis has been used to evaluate the stress distributions and the residual strength under tensile loading of a single- and double-lap repaired composite plate. Key parameters, such as the specimen geometry, stacking sequence and patch thickness, were identified for achieving the optimum performance of the repair (Campilho et al., 2005). In terms of experimental measurement, double-lap joints with both aluminum and steel were investigated experimentally using neutron diffraction and moiré interferometry, and numerically with 2- and 3-dimensional finite element methods (Ruiz et al., 2006). Furthermore, a B-Spline analysis method has been used to evaluate moiré interferometry measurement results of laminated composite joints. It was concluded that, in regions away from the bond line, the through-thickness interlaminar normal strain can be amplified by the presence of the resin used in replicating the grating (Mollenhauer et al., 2008).

\* Corresponding author. Tel.: +886 3 2118800x5743; fax: +886 3 2118346.

E-mail address: [mytsai@mail.cgu.edu.tw](mailto:mytsai@mail.cgu.edu.tw) (M.Y. Tsai).

From this study of the literature, it is concluded that the fundamental mechanics of laminated composite double-lap joints are not well understood, and there is a lack of full-field experimental data. However, an understanding of the mechanics of the double-lap joint is crucial in the application of this jointing technique to laminated composite structures. In the present study, double-lap joints with unidirectional  $[0]_{16}$  and quasi-isotropic  $[0/90/-45/45]_{2s}$  composite adherends and corresponding,  $[0]_8$  and  $[0/90/-45/45]_s$ , straps, under tensile loading, are investigated experimentally, numerically and analytically.

**2. Experimental analysis**

The geometry and materials used in the double-lap test specimens are shown in Fig. 1. The geometry of the test specimen is similar to that specified in ASTM D3528 for an isotropic adherend. Prior to the bonding, the bonding surfaces of the panels were abraded using medium-grit emery papers and then degreased with acetone. The panels were bonded with a film adhesive of EA9628NW manufactured by the Dexter Corporation. The regions of interest (shear area) and extremities of adherend and strap are identified by a circle and expanded in Fig. 1.

Moiré interferometry (Post et al., 1993) was employed to measure in-plane surface deformation of the specimen test section. The high-frequency (1200 lines/mm) cross-diffraction specimen grating was replicated on the edge surface of the overlap region, shown in Fig. 2, with a very thin adhesive (less than 25 μm thick). The specimens were tested in Tinius Olson test machines equipped with a portable achromatic interferometer. The achromatic interferometer developed by Czarnek (1990) has a vibration-insensitivity feature allowing the moiré interferometry experiment to be performed in a conventional test machine. This system also permits simultaneous measurement of  $u$  and  $v$  (horizontal and vertical) displacements needed for determining the shear deformation of the loaded body. The  $u$  and  $v$  displacements can be given as

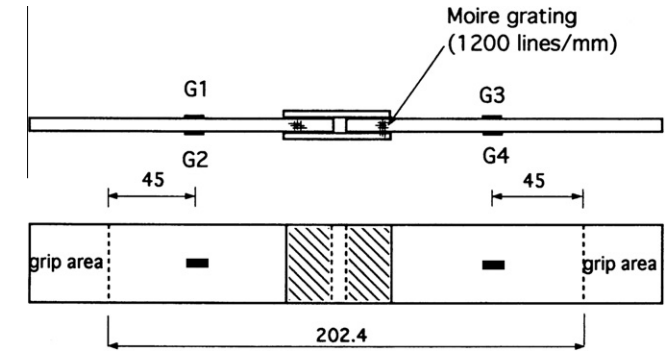


Fig. 2. Moiré grating replication on the edge surface of the double-lap joint and strain gauges (G1–G4) on the surface of the specimen.

$$u(x,y) = \frac{1}{f} N_x(x,y), \tag{1}$$

$$v(x,y) = \frac{1}{f} N_y(x,y), \tag{2}$$

where  $f$  is frequency of a virtual reference grating, 2400 lines/mm in the present system, which is twice the frequency of the specimen grating.  $N_x$  and  $N_y$  are fringe orders with respect to  $u$  and  $v$  displacements, respectively. Thus, one moiré fringe represents 0.417 μm displacement in the current system. Strain components can be obtained by directly differentiating the displacements with respect to coordinates  $x$  and  $y$  as shown:

$$\varepsilon_x = \frac{\partial u}{\partial x} = \frac{1}{f} \left( \frac{\partial N_x}{\partial x} \right), \tag{3}$$

$$\varepsilon_y = \frac{\partial v}{\partial y} = \frac{1}{f} \left( \frac{\partial N_y}{\partial y} \right), \tag{4}$$

$$\gamma_{xy} = \frac{\partial u}{\partial y} + \frac{\partial v}{\partial x} = \frac{1}{f} \left( \frac{\partial N_x}{\partial y} + \frac{\partial N_y}{\partial x} \right). \tag{5}$$

Prior to the moiré data recording, back-to-back strain gauges (G1/G2 and G3/G4 in Fig. 2) remote from the joint were used to monitor the loading condition, in order to assure load alignment. Typical strain gauge responses shown in Fig. 3 indicate that the specimens are properly loaded without significant loading eccentricity. The moiré displacement fields for these composite double-lap joints were determined at load levels within which the adhesive still remained linear and elastic.

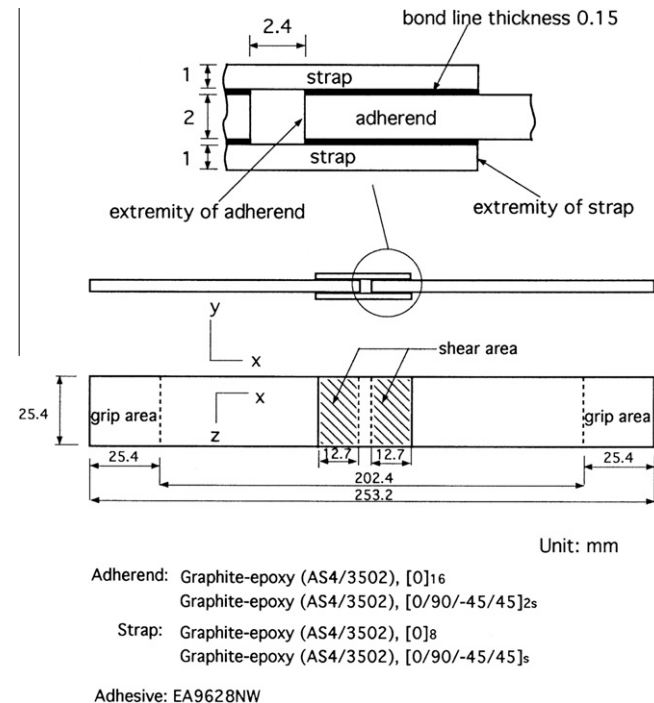


Fig. 1. Geometry and materials of the double-lap test specimens, as per ASTM D-3528 standard.

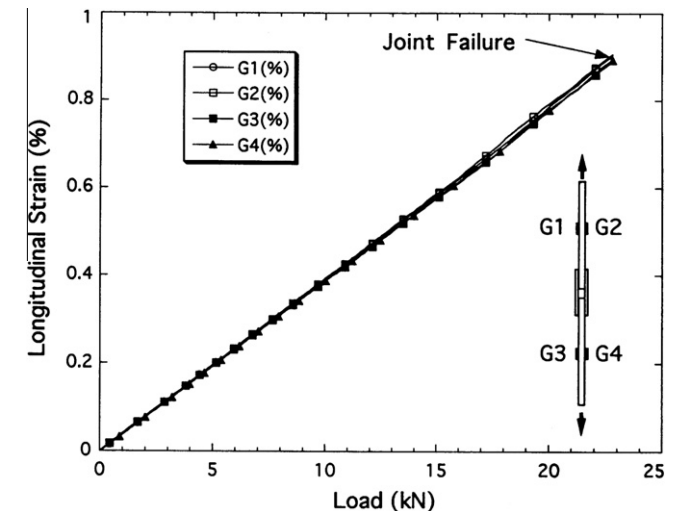


Fig. 3. Typical longitudinal strain responses from strain gauges for the test specimen under tensile loading.

### 3. Numerical and theoretical analyses

To confirm the experimental results and thus understand the mechanics of these laminated composite double-lap joints, two-dimensional linear-elastic finite element analyses (FEM) were performed. ABAQUS, a commercial finite element code, was used in this analysis. The geometry, boundary conditions, and element meshes of the finite element model for the double-lap joint are shown in Fig. 4. Two material cases were analyzed: unidirectional and quasi-isotropic composite joints. Two planes of symmetry exist in this model so that only one quarter of the joint is modeled. The planes of symmetry are specified as roller boundary conditions. The plane strain condition was adopted for simulation of the middle plane or the interior planes away from the free edge surfaces (which suffer three-dimensional free-edge effects (Tsai and Morton, 1995)). Constant-strain (stress) elements (linear displacement elements) were applied to the entire model with two elements across the thickness of the adhesive and one element for each lamina in the laminated adherends. In each lamina, the mechanical properties: elastic moduli  $E_1 = 137$  GPa and  $E_2 = 9.86$  GPa, Poisson ratio  $\nu_{12} = 0.29$ , and shear modulus  $G_{12} = 4.83$  GPa were applied with 1 and 2 representing fiber and matrix directions, respectively. For the adhesive, values  $E_c = 2.38$  GPa and  $\nu_c = 0.32$  were used, being those from the manufacturer's data for EA9628NW epoxy. It is noted that the  $45^\circ$  and  $-45^\circ$  laminae in the two-dimensional models cannot be differentiated in this analysis. Since the nodal stress (or strain) values were calculated by averaging the element nodal values from the adjacent elements, the values of stress (or strain) along the centerline of the adhesive are approximately equal to the average values across the thickness of the adhesive.

For the theoretical analysis, the improved shear-lag based solutions for double-lap joints proposed by Tsai et al. (1998) were used. The double-lap joint geometry and material parameters are shown in Fig. 5. The length of the overlap is  $2c$ . The thicknesses of the outer and inner adherends are  $t_o$  and  $t_i$ , respectively.  $E_o$  and  $G_o$  are the longitudinal elastic and transverse shear moduli of the outer adherends, while  $E_i$  and  $G_i$  are the corresponding properties of the inner adherend.  $G_c$  and  $\eta$  are the adhesive shear modulus and thickness, respectively.  $T$  is the applied force per unit width.  $\tau_{avg}$  is the average adhesive shear stress over the bond line. Thus

$$\tau_{avg} = \frac{1}{2c} \int_{-c}^c \tau_o dx = \frac{T}{4c}, \quad (6)$$

where  $\tau_o$  is the adhesive shear stress, given by

$$\tau_o = A \sinh(\beta x) + B \cosh(\beta x), \quad (7)$$

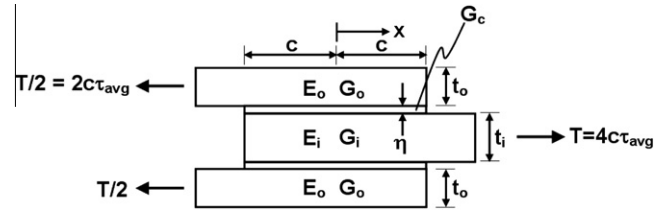


Fig. 5. Geometry and material parameters of the double-lap joint.

where

$$B = \frac{\beta c \tau_{avg}}{\sinh(\beta c)}; \quad (8)$$

$$A = \frac{\beta c \tau_{avg}}{\cosh(\beta c)} \left[ \frac{1 - \frac{E_i t_i}{2E_o t_o}}{1 + \frac{E_i t_i}{2E_o t_o}} \right]; \quad (9)$$

and

$$\beta^2 = \frac{\frac{G_c}{\eta} \left( \frac{2}{E_i t_i} + \frac{1}{E_o t_o} \right)}{\left[ 1 + \frac{G_c}{\eta} \left( \frac{t_i}{6G_i} + \frac{t_o}{3G_o} \right) \right]}. \quad (10)$$

The parameter  $\beta$  can be redefined using two parameters  $\lambda$  (an elongation parameter) and  $\alpha$  (a shear deformation parameter), as

$$\beta^2 = \alpha^2 \lambda^2, \quad (11)$$

where

$$\lambda^2 = \frac{G_c}{\eta} \left( \frac{2}{E_i t_i} + \frac{1}{E_o t_o} \right), \quad (12)$$

and

$$\alpha^2 = \left[ 1 + \frac{G_c}{\eta} \left( \frac{t_i}{6G_i} + \frac{t_o}{3G_o} \right) \right]^{-1}. \quad (13)$$

The closed-form solution proposed by Volkersen (1938) and de Bruyne (1944) can be recovered by assuming that adherend shear deformations are zero, or that adherend shear moduli  $G_i$  and  $G_o$  are infinitely large, i.e.  $\alpha = 1$ .

The double-lap joints with unidirectional and quasi-isotropic composite adherends were analyzed using these theoretical solutions. The geometrical parameters are:  $2c = 12.7$  mm,  $t_o = 1$  mm,  $t_i = 2$  mm, and  $\eta = 0.15$  mm. The relevant material properties are: for the unidirectional adherends joint,  $E_o = E_i = 137$  GPa,  $G_o = G_i = 4.83$  GPa; for the quasi-isotropic adherends joint,  $E_o = E_i = 50$  GPa,  $G_o = G_i = 3.80$  GPa; and for adhesive  $G_c = 0.91$  GPa. Noted that

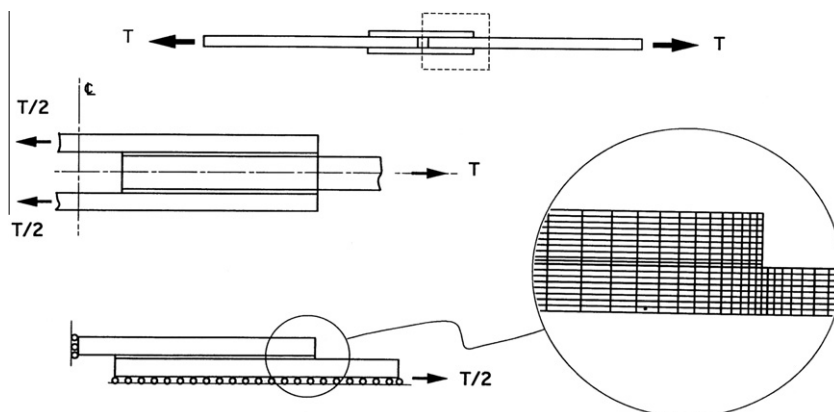


Fig. 4. Boundary conditions and element meshes in the finite element model.

$G_o$  and  $G_i$  for the quasi-isotropic adherend, were calculated by averaging  $G_o$  or  $G_i$  for all laminae. In other words,  $0^\circ$ ,  $90^\circ$ ,  $-45^\circ$  and  $45^\circ$  layers are determined from the lamina three-dimensional (3-D) constitutive stiffness matrix. The value of the adhesive shear modulus  $G_c$  is calculated from  $E_c$  and  $\nu_c$ .

#### 4. Results and discussion

Typical moiré fringe patterns obtained from the experiments for the unidirectional and quasi-isotropic joints under the similar load are shown in Figs. 6 and 7, respectively. The  $u$  and  $v$  fields represent the horizontal and vertical displacement fields, respectively. In

Fig. 6, it is apparent that the fringe patterns for  $u$  and  $v$  fields are smooth and almost symmetrical about the mid-plane of the adherend for the unidirectional joint. The  $u$ -displacement gradients in the  $x$  direction (i.e.  $\partial u/\partial x$ ), representing strain  $\epsilon_x$ , in the adherend are relatively large near the beginning of the joint, but are very small (close to zero) at the free extremity of the adherend, and correspondingly for the straps of the joint. This is consistent with the longitudinal force in the adherend being completely transferred to the two outer straps via the adhesive layers through the adhesive shear stresses. The adhesive at and near the extremities of the adherend and strap carry relatively large shear stresses which result in the large shear strain (the large  $u$  fringe gradient in the  $y$  direction). The adhesive shear strains are relatively small at the

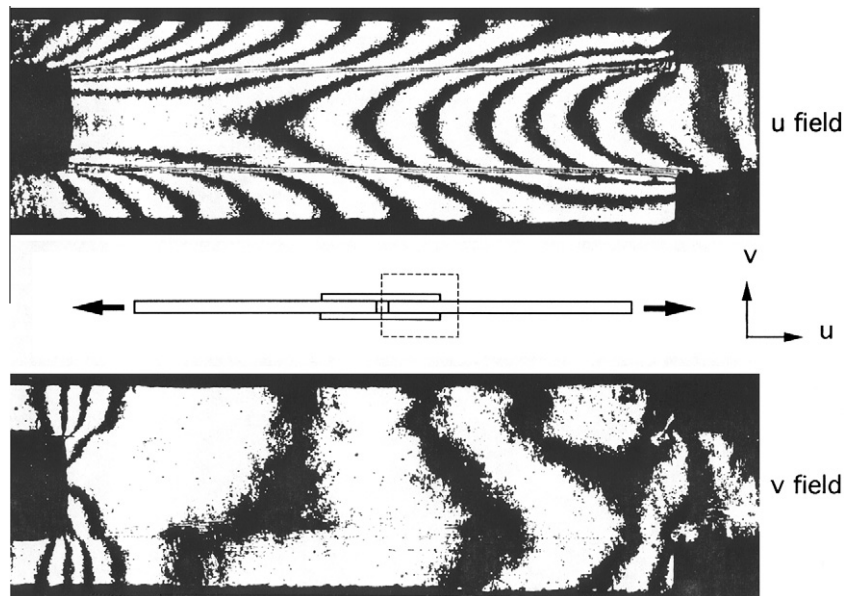


Fig. 6. Typical moiré fringe patterns for a unidirectional  $([0]_{16})$  double-lap joint under  $P = 3478$  N (782 lbs), about 17% load to failure.

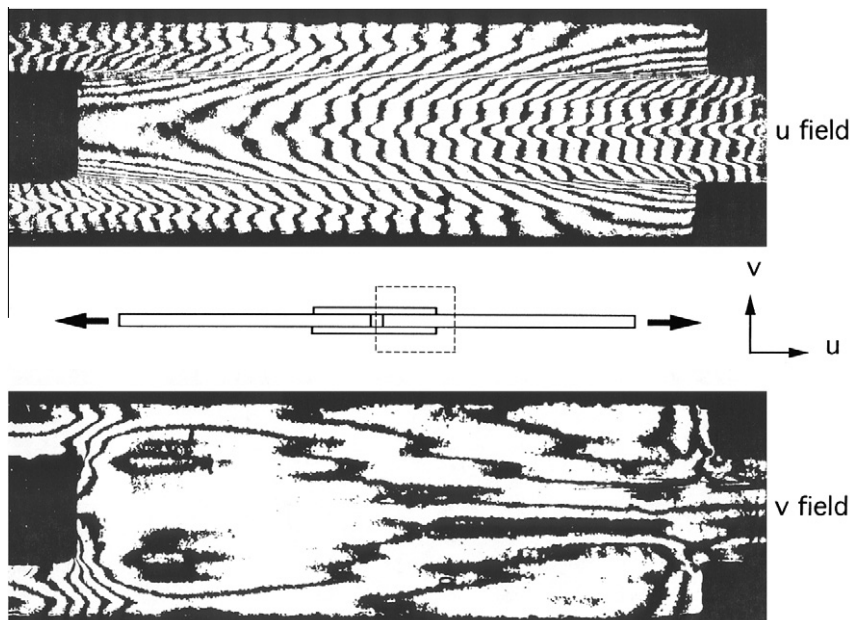


Fig. 7. Typical moiré fringe patterns for a quasi-isotropic  $([0/90/-45/45]_{2s})$  double-lap joint under  $P = 3456$  N (777 lbs), about 16% load to failure.

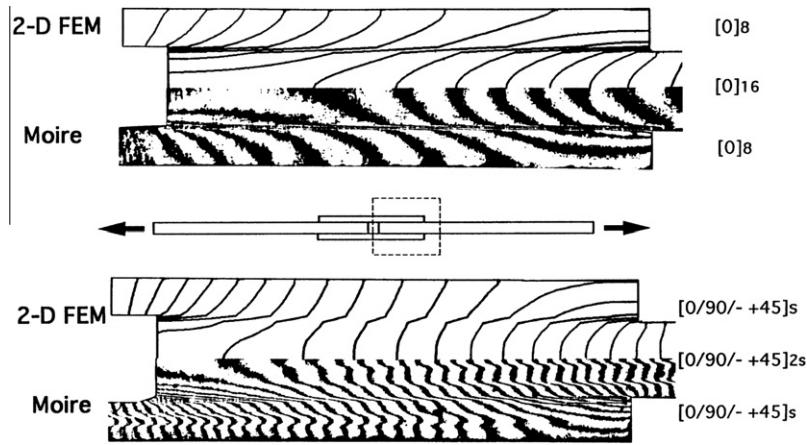


Fig. 8. Comparisons of moiré- and FEM-determined horizontal ( $u$ -) displacement fields for unidirectional and quasi-isotropic double-lap joints. (Note: the fringe pattern for the quasi-isotropic joint from FEM is presented by every two fringes).

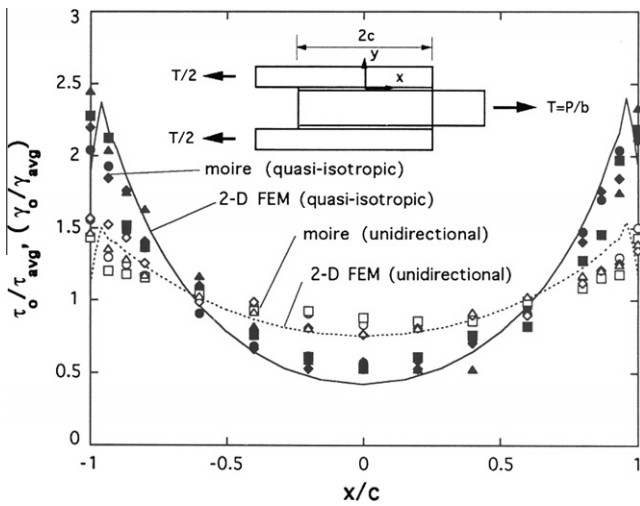


Fig. 9. Comparison of moiré- and FEM-determined normalized adhesive shear strain (stress) distributions for unidirectional and quasi-isotropic double-lap joints.

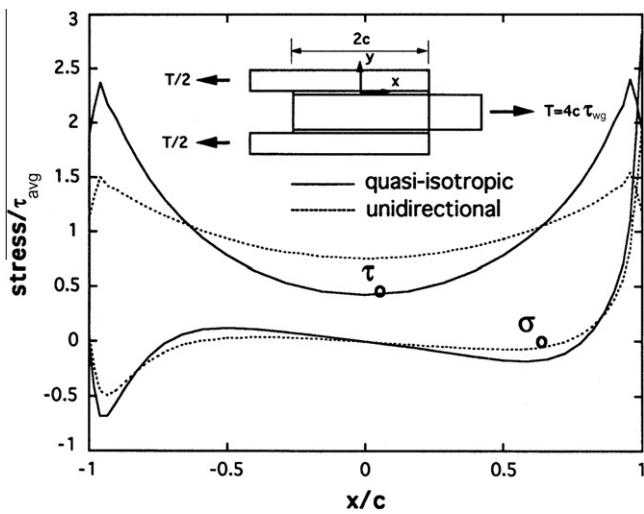


Fig. 10. FEM-determined normalized adhesive shear and peel stress distributions for unidirectional and quasi-isotropic double-lap joints.

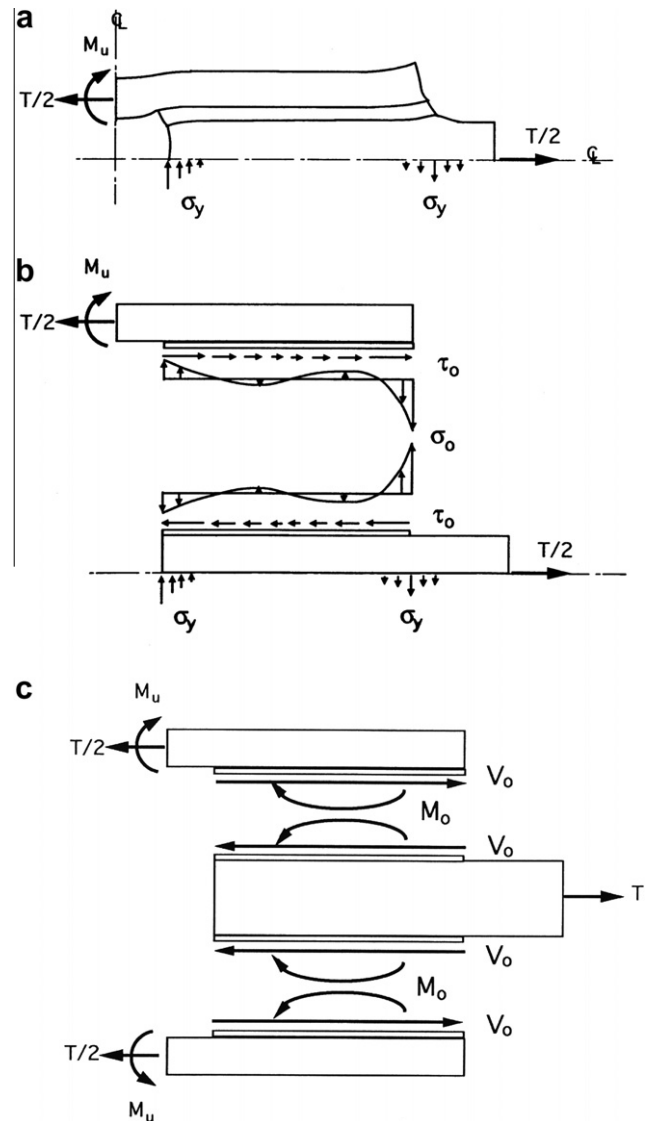


Fig. 11. (a) Deformation of a quarter of double-lap joint, (b) free-body diagram of a quarter of a double-lap joint and (c) free-body diagram for half of a double-lap joint.

centre of the overlap but large at the both ends. The curved fringes in the straps and adherend imply the presence of significant shear deformations due to low shear stiffness of the composite adherend and straps. For the  $v$  field, the displacement gradients in the  $y$  direction (i.e.  $\partial v/\partial y$ ), representing strain  $\varepsilon_y$ , are very small in the adherend, straps and adhesive, compared with the other strains ( $\varepsilon_x$  and  $\gamma_{xy}$ ). Note that there are compressive strains  $\varepsilon_y$  in the adhesive near and at the extremity of the adherend. These compressive  $\varepsilon_y$  will be discussed later.

The fringe patterns in the quasi-isotropic composite joint experiment, shown in Fig. 7, are different from those in the unidirectional joint case. The  $u$ -field fringes in the quasi-isotropic joints have a degree of waviness in both the adherend and strap. It is apparent that this waviness occurs between layers with off-axis fibers ( $\pm 45^\circ$  layers in this case). These off-axis layers have an in-plane stretching-shear coupling characteristic that results in interlaminar shear stresses near and on the free surfaces due to a three-dimensional stress state. These interlaminar shear stresses generate the fringe waviness between the layers with off-axis fibers. This

phenomenon has been discussed in detail in the reference (Tsai and Morton, 1995). Apart from the fringe waviness, the values of  $\varepsilon_x$  in the adherend and straps are higher in the quasi-isotropic joint, due to a lower longitudinal stiffness than that of the unidirectional joint, under similar load. The shear deformations in the adherend and straps near the extremities, for the quasi-isotropic joint, are about twice those of the unidirectional joint, even though the shear modulus of the quasi-isotropic joint is slightly lower than that of the unidirectional joint.

To confirm the data derived from the experiments and provide insight into mechanics of the joints, the deformations and adhesive strain distributions obtained from the finite element analyses are compared with the experimental data. The full-field displacements determined from the moiré experiments and FEM are shown in Fig. 8 for unidirectional and quasi-isotropic joints. Note that for illustrative purposes the fringe patterns for the quasi-isotropic joint from the FEM are printed by every two fringes. It is clear that for both unidirectional and quasi-isotropic joints the fringe patterns from the FEM are very consistent with those from the moiré

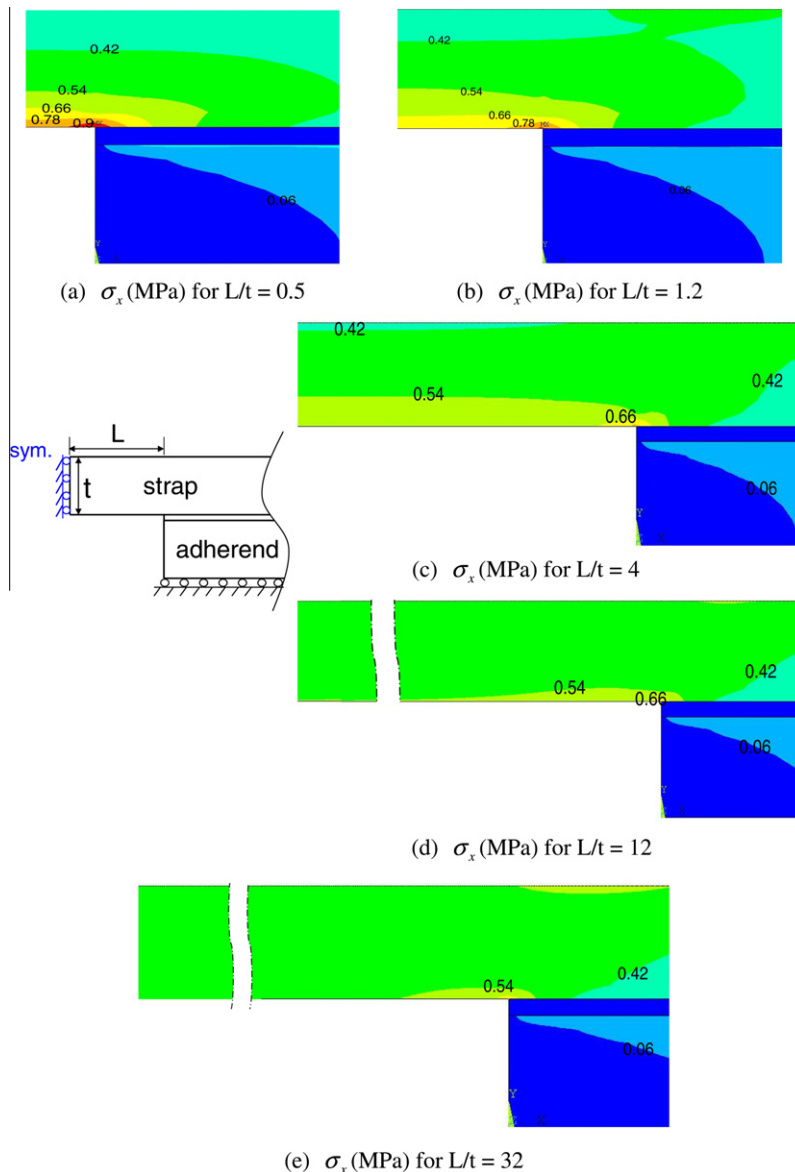


Fig. 12.  $\sigma_x$  stress distributions for unidirectional joints with the different length of the straps (a)  $L/t = 0.5$ , (b)  $L/t = 1.2$ , (c)  $L/t = 4$ , (d)  $L/t = 12$ , and (e)  $L/t = 32$  from FEM for  $T = 1$  N/mm.

experiments, except for the local waviness in the quasi-isotropic joint. As mentioned above, this local waviness, which is caused by the presence of off-axis plies, is three-dimensional (free-edge) phenomena occurring only near and on the free surfaces (Tsai and Morton, 1995; Czarnek et al., 1983), and which cannot be predicted using a two-dimensional analysis. Comparisons of the adhesive shear distributions obtained from both analyses are shown in Fig. 9 for the unidirectional and quasi-isotropic joints. It is clear that the adhesive shear strain (stress) distributions from both analyses are in very good agreement for most regions of the bond line, except in the very small zones near the extremities of the adherend and strap. The FEM predicts that the shear stress distributions have a tendency to drop to zero at the extremities in order to satisfy the free shear stress at the free ends. On the other hand, the moiré experiments cannot capture this trend due to the resolution and averaging scheme used in obtaining the adhesive strain data.

The adhesive peel (transverse normal) stress is an important component, possibly resulting in the initiation of joint failure. Since the maximum peel stress occurs in the two-dimensional region (extending from the centre-plane of the joint some way in the width-wise direction), the free surface measurement of moiré experiment will not capture it. However, the two-dimensional finite element model validated by experimental solutions can be used to determine the adhesive peel stresses. The normalized adhesive shear and peel stress distributions from the FEM are shown in Fig. 10 for the unidirectional and quasi-isotropic joints. It is apparent that for both joints large tensile peel stresses occur near and at the extremity of strap ( $x = c$ ), while medium compressive peel stresses appear near and at extremity of the adherend ( $x = -c$ ). It may also be observed that, unlike the adhesive shear stress, the adhesive peel distributions in most of the bond line are not affected significantly by the material properties of the adherend and strap, except in the small region near the extremity of the strap. In this small region, the value of the maximum peel stress is higher in the quasi-isotropic joint than in the unidirectional joint.

From the experimental observations and the numerical simulations, the deformations and mechanics of the double-lap joint can be represented as shown in Fig. 11. Fig. 11(a) presents the deformation of the double-lap joint with two planes of symmetry (mid-planes of the joint and the adherend). It is noted that there are transverse normal stresses ( $\sigma_y$ ) in the mid-plane of the adherend and a strap moment,  $M_u$ , in the centre line of the strap, as well as the longitudinal force  $T/2$ . This force and moment equilibrium system results in the compressive deformations near the extremity of the adherend and the tensile deformations near the extremity of the strap. The detailed free-body diagram for the quarter of the joint is represented in Fig. 11(b). The adhesive stress system ( $\sigma_o$  and  $\tau_o$ ) is in equilibrium with the  $M_u$  and  $T/2$  in the strap element or with  $\sigma_y$  and  $T/2$  in the adherend element. Let adhesive moment ( $M_o$ ) be defined as

$$M_o = \int_{-c}^c \sigma_o x dx \quad (14)$$

and adhesive shear ( $V_o$ ) be

$$V_o = \int_{-c}^c \tau_o dx. \quad (15)$$

The free-body diagram for a half of the double-lap joint is shown in Fig. 11(c). Based on force and moment equilibrium, then

$$V_o = \frac{T}{2}; \quad (16)$$

$$M_u + M_o = \frac{T}{2} \left( \frac{t + \eta}{2} \right), \quad (17)$$

where  $t$  is a thickness of the strap and  $\eta$  the thickness of the adhesive layer. Since  $M_u$  is a self-equilibrating moment it is easy to overlook it in the analysis. If  $M_u$  were omitted, then  $M_o$  becomes

$$M_o = \frac{T}{2} \left( \frac{t + \eta}{2} \right) \quad (18)$$

and Eq. (18) would result in different the adhesive stress distributions.

The effect of the strap moment  $M_u$  (and the length of strap) on the adhesive stress distribution was further investigated in a finite element analysis. In Fig. 12, it is apparent that  $\sigma_x$  stress distributions for unidirectional joints depend upon the length of the strap particularly along the line of symmetry and near the end of the adherend. The  $\sigma_x$  stress distributions along line ab (line of symmetry of the strap) and line cd (near the end of adherend) are plotted in Fig. 13(a) and (b), respectively, for the range of strap lengths  $L/t = 0.5-32$ . It can be seen from Fig. 13(a) that  $M_u$  (resulting from the non-uniform  $\sigma_x$ ) decreases with the length of the strap. As a result, the bending moment near the end of adherend, shown in Fig. 13(b), also decreases as the strap becomes longer. Note that the cases of  $L/t = 32$  and 1.2 represent the specimens type A and B suggested by ASTM D3528 (1981). The effect of the  $M_u$  on the adhesive stress distribution is illustrated in Fig. 14. The presence of the  $M_u$  causes an increase in the maximum adhesive shear in Fig. 14(a) and a decrease in the maximum compressive adhesive peel at the end of the adherend in Fig. 14(b), but does not affect either stress at the end of the strap. Meanwhile, as the length of the strap gets larger (especially beyond  $L/t = 32$ ), both the adhesive shear and peel stress distributions converge towards those for the cases with uniform stress and concentrated force boundary conditions, i.e. those without the  $M_u$ . The above results relate to unidirectional double-

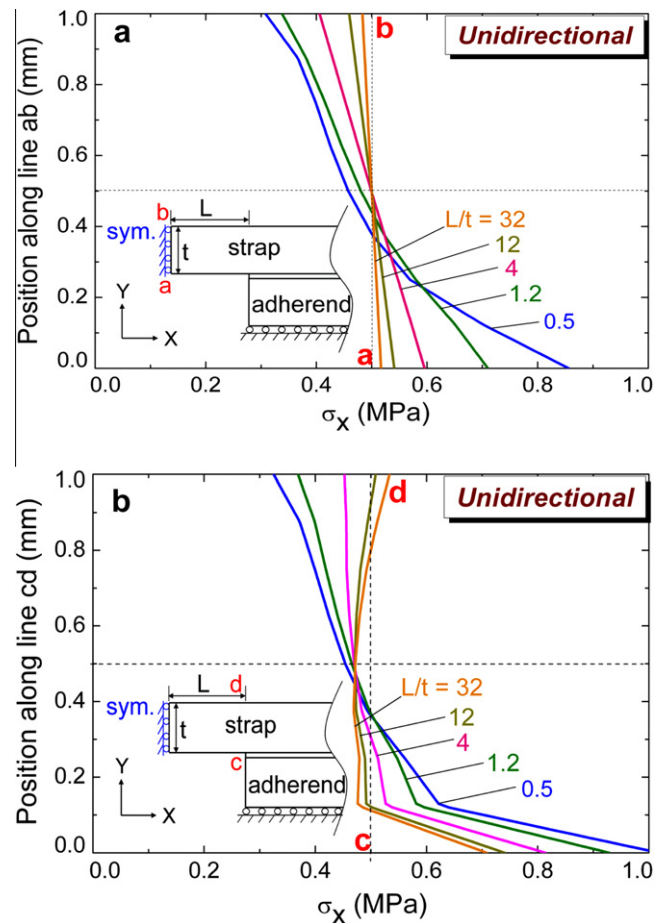


Fig. 13.  $\sigma_x$  stress distributions for unidirectional joints (a) along line ab (symmetric line), and (b) along line cd (near the end of adherend) with different strap length  $L/t = 0.5-32$  from FEM for  $T = 1$  N/mm.

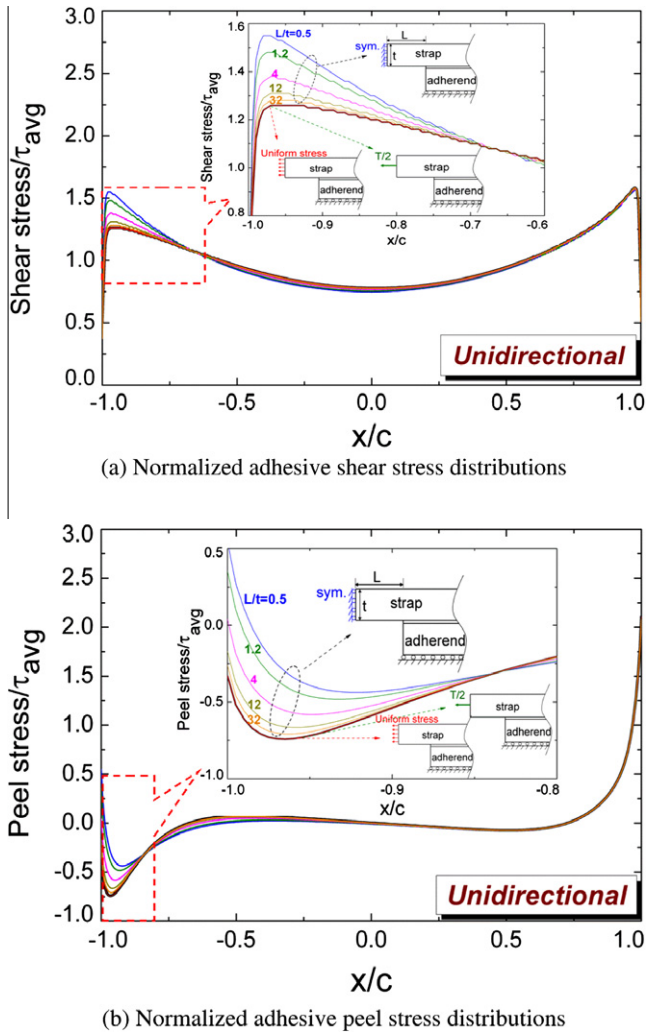


Fig. 14. FEM-determined (a) normalized adhesive shear and (b) peel stress distributions for unidirectional double-lap joints with different strap length  $L/t = 0.5-32$  with different boundary conditions: symmetrical, uniform stress, and concentrated force.

lap joints. However, for quasi-isotropic joints, a similar mechanism was found, but the stress values were different, of course. A similar result was reported by Oterkus et al. (2006), in which the influence of the gap (equivalent to  $L/t$ , here) between the center adherends was studied. They found that the compressive adhesive peel stress along the inner edge increases with increasing gap size (that is, in agreement with the present findings), while the adhesive shear is not sensitive to it. The latter finding is not consistent with the present results. This difference in the adhesive shear is caused by ignoring the shear deformation in the adherend, a recognized limitation of the Kirchhoff theory used by Oterkus et al. Since the peel stresses are primarily determined by the normal (bending, tensile and compressive) stiffnesses, which are modelled quite well in the Oterkus paper, there is agreement with the present work.

Available classical solutions for the double-lap joint, Volkersen (1938) and de Bruyne (1944) and Tsai et al. (1998) were examined in terms of their assumptions and predictions, and compared with the present experimental observations. Volkersen and de Bruyne modeled the adherend and strap as bars which are allowed to deform only in the longitudinal direction and uniformly through the thickness of the adherend and strap. The adhesive layer was considered as a shear spring carrying only the shear stresses needed to transfer the longitudinal forces from the adherend to the straps.

It is shown in the experiments that these assumptions of zero adherend (and strap) shear deformations in the theory are not valid in the joints with laminated composite adherends. As a result, the theory predicted maximum values of the adhesive shear stress (strain) about 33% higher than those in the experiment, shown in Fig. 15. However, Tsai, Oplinger and Morton solution, with modification to include the adherend and strap shear deformations, appears to provide a very good prediction of the normalized adhesive shear strain (stress) distributions for both joints, shown in Fig. 16.

Typical failure modes of the unidirectional  $([0]_{16})$  and quasi-isotropic  $([0/90/-45/45]_{2S})$  double-lap joint specimens under tensile loads were observed and sketched in Fig. 17. It is apparent that on one strap the unidirectional joint has suffered cohesive failure, while the quasi-isotropic joint undergoes delamination at the first ply ( $0^\circ$  layer). Furthermore, on the other strap both joints have a mixed tensile and shear failure mode at the interfaces between the adherend and adhesive, and between the strap and adhesive. Based on observation during the test, the cohesive failure in the

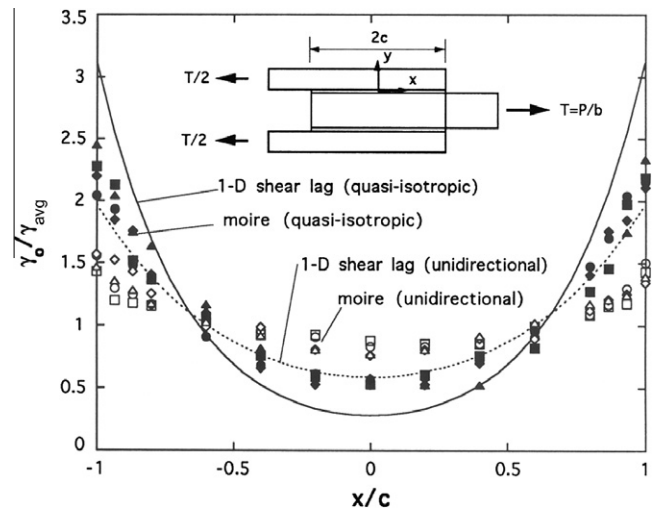


Fig. 15. Comparison of moiré- and 1-D Volkersen and de Bruyne-determined normalized adhesive shear strain (stress) distributions for unidirectional and quasi-isotropic double-lap joints.

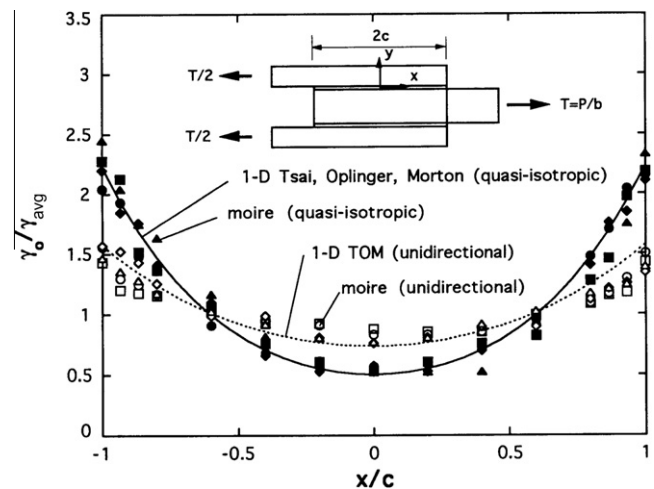


Fig. 16. Comparison of moiré- and 1-D Tsai, Oplinger, Morton-determined normalized adhesive shear strain (stress) distributions for unidirectional and quasi-isotropic double-lap joints.

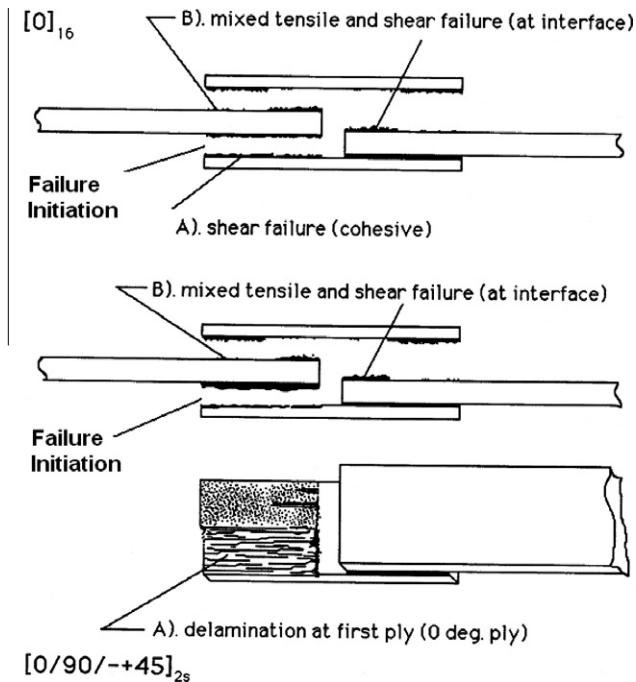


Fig. 17. Typical failure modes of the unidirectional  $[0]_{16}$  and quasi-isotropic  $[0/90/-45/45]_{2s}$  double-lap joint specimens under tensile loads.

unidirectional joint and the delamination at the first ply in the quasi-isotropic joint occur first by failure initiation at the end of the strap, and determine the maximum failure load. It seems that unlike the unidirectional joint the interlaminar stresses in the quasi-isotropic joint play a significant role in failure initiation.

## 5. Conclusions

The stress distributions and mechanics of the laminated composite double-lap joints with unidirectional and quasi-isotropic adherends have been derived on the basis of the results obtained from experimental, numerical and theoretical analyses. Experimental and finite element results suggest that the displacement fields obtained from both analyses are in a good agreement, respectively, for both joints, except for a fringe waviness, due to the three-dimensional free-edge phenomena, in the quasi-isotropic composite joint. Furthermore, the laminated composite double-lap joints have significant adherend shear deformations, which have been neglected in the theoretical modelling. It is also observed that there are transverse normal stresses in the mid-plane of the adherend and a strap moment in the mid-plane of the strap, as well as the longitudinal force. This force and moment equilibrium system results in the compressive deformations in the transverse direction near the extremity of the adherend and the tensile deformations near the extremity of the strap. It is also found that a strap moment, dependent on the length of the strap, would cause an increase in the maximum adhesive shear and a decrease in the maximum compressive adhesive peel at the end of the adherend but does not affect either stress at the end of the strap for both joints. One-dimensional shear-lag closed-form solu-

tions taking into account the adherend shear deformations can provide very good prediction not only of the adhesive shear distributions, but also the maximum values of adhesive shear strain (stress). It is also noted that the normalized adhesive shear strain (stress) distributions for both joints are not uniform. The non-uniformity of adhesive shear for the quasi-isotropic joint is greater than that for the unidirectional joint. This difference of shear non-uniformity is mainly attributed to the different longitudinal stiffness. The typical failure initiations for both joints were also documented and found to occur at the end of the strap with the cohesive failure in the unidirectional joint and with the delamination at the first ply in the quasi-isotropic joint.

## Acknowledgements

The financial support from the Federal Aviation Administration, USA under the contract USDOT/FAA 93-G-064, and from the National Science Council, Taiwan, ROC, under the contract NSC88-2216-E-182-002 is greatly appreciated. The authors also would like to express their thanks to Dexter Corporation for providing the adhesive material for this study and Mr. P. S. Huang for performing part of finite element analysis.

## References

- ASTM D3528, 1981. Standard test method for strength properties of double-lap shear adhesive joints by tension loading. Annual Book of ASTM Standards.
- Bahei-El-Din, Y.A., Dvorak, G.J., 2001. New designs of adhesive joints for thick composite laminates. *Composites Science and Technology* 61, 19–40.
- Campilho, R.D.S.G., de Moura, M.F.S.F., Domingues, J.J.M.S., 2005. Modeling single and double-lap repairs on composite materials. *Composites Science and Technology* 65, 1948–1958.
- Czarnek, R., Post, D., Herakovich, C.T., 1983. Edge effects in composites by moiré interferometry. *Experimental Techniques* 7 (1), 18–21.
- Czarnek, R., 1990. High sensitivity moiré interferometry with compact achromatic interferometer. *Optics and Lasers in Engineering* 13, 99–115.
- Chalkley, P., Rose, F., 2001. Stress analysis of double-strap bonded joints using a variational method. *International Journal of Adhesion and Adhesives* 21 (3), 241–247.
- de Bruyne, N.A., 1944. The strength of glued joints. *Aircraft Engineering* 16, 115–118.
- Ishii, K., Imanaka, M., Nakayama, H., Kodama, H., 1999. Evaluation of the fatigue strength of adhesively bonded CFRP/metal single and single-step double-lap joints. *Composites Science and Technology* 59, 1675–1683.
- Mollenhauer, D.H., Fredrickson, B.M., Schoeppner, G.A., larve, E.V., Palazotto, A.N., 2008. Moiré interferometry measurements of composite laminate repair behavior: influence of grating thickness on interlaminar response. *Composites: Part A* 39, 1322–1330.
- Oterkus, E., Barut, A., Madenci, E., Smeltzer, S.S., Ambur, D.R., 2006. Bonded lap joints of composite laminates with tapered edges. *International Journal of Solids and Structures* 43 (6), 1459–1489.
- Post, D., Han, B., Ifju, P., 1993. *High Sensitivity Moiré Experimental Analysis for Mechanics and Materials*. Springer-Verlag, New York.
- Ruiz, P.D., Jumbo, F., Seaton, A., Huntley, J.M., Ashcroft, I.A., Swallowe, G.M., 2006. Numerical and experimental investigation of three-dimensional strains in adhesively bonded joints. *Journal of Strain Analysis for Engineering Design* 41 (8), 583–596.
- Tong, L., Soutis, C., 2003. *Recent Advances in Structural Joints and Repairs for Composite Materials*. Kluwer Academic Publisher, The Netherlands.
- Tsai, M.Y., Oplinger, D.W., Morton, J., 1998. Improved theoretical solutions of adhesive joints. *International Journal of Solids and Structures* 35 (12), 1163–1185.
- Tsai, M.Y., Morton, J., 1995. Experimental and numerical studies of a laminated composite single-lap adhesive joint. *Journal of Composite Materials* 29 (9), 1254–1275.
- Volkersen, O., 1938. Die Niekraftverteilung in Zugbeanspruchten mit konstanten Laschenquerschnitten. *Luftfahrtforschung* 15, 41–47.